Statistical approach of factors controlling drainage network patterns in arid areas. Application to the Eastern Anti Atlas (Morocco)

Tarik Bouramtane, Suzanne Yameogo, Meryem Touzani, Abdessamad Tiouiouine, M'Hamed El Janati, Jamila Ouardi, Ilias Kacimi, Vincent Vallès, Laurent Barbiero

Statistical approach of factors controlling drainage network patterns in arid areas. Application to the Eastern Anti Atlas (Morocco)

Tarik Bouramtane[1], Suzanne Yameogo[2], Meryem Touzani[1], Abdessamad Tiouiouine[1], M'hamed El Janati[1], Jamila Ouardi[3], Ilias Kacimi[1], Vincent Valles[4], Laurent Barbiero[5]

1 Geoscience, Water and Environment Laboratory, Faculty of Sciences, Mohammed V University, Avenue Ibn Batouta, Rabat Morocco.
2 Université de Ouagadougou (Pr J. Ki-Zerbo), B.P. 7021 Ouagadougou 03, Burkina Faso.
3 Regional Centre for Education and Training Professions, El Jadida
4 Université d'Avignon et des Pays de Vaucluse, UMR EMMAH
5 IRD, CNRS, Université de Toulouse, Observatoire Midi-Pyrénées, UMR 5563, Géoscience Environnement Toulouse, 14 Av. E. Belin, 31400 Toulouse

Abstract:

Several studies have revealed that the complexity in the distribution of drainage network patterns is not random and controlled by major parameters, variable in space but also throughout geological time. Drainage networks in the Eastern Anti-Atlas of Morocco consist of complex spatial arrangements with various types of patterns, such as trellis, angular, dendritic and parallel. The objective was to distinguish, quantify and rank the relationship that may exist between the different drainage networks patterns, geology and geomorphology. A total of 230 basins were extracted from the ASTER-GDEM Elevation Data (USGS), which were assigned 16 parameters reflecting their topography, morphometry, slope and geology. The statistical treatment of the dataset (16 variables x 230 observations) was carried out through principal component analysis (PCA), linear discriminant analysis (LDA) and agglomerative hierarchical clustering (AHC), in order to investigate the complexity of drainage network patterns and their distribution. The PCA showed that the topographical, slope and geological parameters, i.e. primarily the parameter associated with structural control, best explains the variation in the type of the drainage pattern. The LDA made it possible to distinguish between the four types of drainage patterns with a success rate of 90%, using 3 discriminant functions that were better correlated with geological and slope parameters. LDA and AHC statistical treatments show confusion between the parallel, trellis and angular patterns, on the one hand, due to similar factors responsible for their formation, and on the other because of transitions phenomenon from one drainage pattern to another over time or space. Such possible drainage network shifting may be explained by the geological events that have occurred in the Eastern Anti Atlas from Lower Mesozoic to the Quaternary.

Keywords: Drainage network patterns, Arid area, Principal Component Analysis, Linear discriminant analysis, Anti-Atlas, Morocco.

1. Introduction

The hydrology of arid regions is a difficult subject to deal, due to scarcity of flows, absence of morphogenic floods, and difficulty in performing a natural chemical or isotopic tracing or a continuous monitoring of the flow. To these characteristics, it is generally necessary to add the scarcity of reliable information on water resources (Gunkel et al., 2015; Mengistu et al., 2019). Due to the violence of rain events, floods represent a real risk in arid regions and their modeling for risk prediction depends partly on knowledge of the type of drainage network (Saidi, 1994; Fink and Knippertz, 2003; Mohammadi et al., 2017; Fels et al., 2018). The scarcity of vegetation in arid zones is a positive aspect that facilitates the study of basins structures by satellite imagery (Jung et al., 2011; Ouarda and Jung, 2015; Jung and Ouarda, 2017). These arid zones are also of great interest because the structure of basins is usually inherited from past geological periods, which can be regarded as recorders of a long geological history and conditions that led to their formation. Understanding the formation of the drainage networks and their evolution over time offers the possibility of deciphering the regional geological chronology (Howard, 1967; Friend et al., 2009), i.e. past tectonic movements and their succession (Brookfield, 2008; Stokes et al., 2008), different geological deformations (Twidale, 1994, 1997; Babault et al., 2012) and regional landscape evolution (Malik and Mohanty, 2007; Abdelkareem and El-Baz, 2015). Inversely, the knowledge of the geological history of a region can help interpret the development of drainage systems (Clarke, 1994; Demoulin, 1998; Schumm et al., 2002; Clark et al., 2004; Twidale, 2004; Malik and Mohanty, 2007; Mejía and Niemann, 2008; Friend et al., 2009; Burbank and Anderson, 2011; Babault et al., 2012). When relevant geological information is available, association of

geology and drainage pattern considerations are frequently used to interpret the geological context without previous mapping (Drury, 2004). The differences in drainage patterns have led geomorphologists to develop classification systems for channel networks and to extract clues and information that reinforce hypothesis on some major geological events. Johnson (1932) conducted the first work on the meaning of drainage patterns, assuming that rivers follow the slope first and then adjust to structure. Zernitz (1932) observed that surface slope and rock resistance determine drainage patterns. This author stated that slope induces the formation of patterns such as dendritic, parallel, radial and distributary, while geological structures (Joints, Faults and folds) produces straight, angular, trellis and annular arrangements. Parvis (1950) expanded this classification system by introducing fifteen modified patterns. Howard (1967) conducted a more comprehensive study, adding new basic patterns and giving them a broader definition. He also suggested that transition patterns could result from changes from one scheme to another over time.

The eastern Anti-Atlas of Morocco (EAA) is characterized by a wide variety of prominent and distinct geological structures, ranging in age from Precambrian to Quaternary. The EAA have suffered several geological events and constraints of various orientations, such as the Hercynian collision between Laurentia and Gondwana responsible for the reactivation of several inherited faults, a rise of the Precambrian basement and a folding of the Paleozoic cover (Robert-Charrue, 2006; Baidder et al., 2016). In this context, deciphering the role of the parameters controlling the development of the various types of drainage network necessarily involves a statistical approach capable of extracting information contained in large databases that combines numerous observations and their characteristics. The objective of this work, carried out in the little known but complex area of the EAA, is to apply and combine various mathematical approaches to study this relationship between the different drainage networks patterns, topography and geology. A large number of parameters is used for the characterization of the area. An approach on individually taken or cross-referenced parameters 2 to 2 is quickly presented, but the complexity of the dataset requires a multivariate statistical approach. The independent sources of variability are studied by principal component analysis (PCA), which allows the information to be concentrated in a smaller number of macroparameters, i.e. the Principal Components. On this basis, hierarchical agglomerative clustering (HAC) allows a comparison of different types of drainage networks. Finally (and especially) a multiparameter linear discriminant analysis (LDA) makes it possible to determine whether it is possible to predict the type of drainage network based on the geological and topographical characteristics of the area, i.e. to verify whether there is a relationship between the environmental characteristics and the type of drainage network.

2. Material and methods

2.1. Study area:

The studied basins are located in the Eastern Anti-Atlas, in southeastern Morocco (Fig. 1). The Anti-Atlas forms a vast anticlinal extending from the Atlantic Ocean South-Westward to Hamada of Guir North-Eastward. The EAA represents sectors of Neoproterozoic paleo continents preserved from the Pan African to Alpine orogenies as recorded in their marginal belts. Intense foldings and overthrustings mark the limits between the Neoproterozoic belts and the surrounding cover (Fig. 1). The EAA region consists of six identifiable sectors (Table 1):

(1) The Bani sector (BS) is a folded Paleozoic cover located southwest of the study area. The term "bani" refers to monoclinal semi-tubular structures from Cambrian to Devonian (Choubert, 1943; Colmenar et al., 2018; Ouanaimi et al., 2018). The Ordovician covers a vast area, with two ridges of hard sandstone, namely the first and second bani, separated by two levels of clay, called Feija and Ktaoua shales, respectively.

(2) The sector of Ougnat-Ouzina axis (OOA) also is referred as the anticlinorium of Taouz in the literature. It is a wide NNW-SSE trend shear zone containing Cambrian anticlinal folded structures (Jbel Taklimt, Jbel Renneg and Jbel Tijekht). Folded Ordovician structural units are also described in the northeastern and southeastern part of this sector (Bou Mays and Amelane-Mech Irdane, the anticlinal units of Shayb Arras and Jbel Tazout), and are separated from each other by synclinal folds of Devonian and Carboniferous age (Ottara and Amessoui synclinals) (Baidder et al., 2016).

(3) The Maider Basin sector (MB), around the Lower Carboniferous Fesou synclinal in the center of the EAA is weakly deformed compared to other sectors. Its western boundary is a monoclinal folds zone, whereas

in the south it is delimited by anticline folds trending E-W to ENE-WSW (Kaufmann, 1998; Robert-Charrue, 2006; Baidder et al., 2016).

(4) The Kem-Kem Domain (KKD) includes a large stony tabular area of Cretaceous deposits, which highlights the partial erosion of sedimentary cover formed by detrital deposits. These formations remain intact, without significant developed structures (Robert-Charrue, 2006; Baidder et al., 2016).

(5) The South-Tafilalt Basin sector (STB) is characterized by the broad Lower Carboniferous Merzouga synclinal with a WNW-ESE trend axis, and parallel to the middle Devonian Erfoud anticlinal located northeast the sector.

(6) The sector of the Saghro-Ougnat axis (SOA) comprises two large inliers, the Saghro and Ougnat Precambrian massifs, which constitute the highest points in the study area, at over 3200 m altitude. This sector is considered as a Pan-African arc (Walsh et al., 2012), separating two significant geological domains, namely the High Atlas in the north and the Sahara of Morocco in the south. The inliers overlie deep faults reactivated on a scale of several kilometres, namely Assif n'Oussif Fault, Boulghzazil-Tinifift Fault, Akrouz Fault and Tizi n'Ressas Fault (Soulaimani et al., 2014). Several volcanic units occur and consist of andesitic to rhyo-dacitic volcanic and volcaniclastic rocks including mainly ignimbrites and tuffs.

BS, MB and STB are lowland areas alternating with Appalachian landforms and mountainous areas in the north. MB and STB are more precisely plains of a synclinal nature. These lowland areas contain basin structures such as the Tazzarine basin in SB, the large fezzou syncline in MB and the Ziz plain in STB with quaternary deposits.

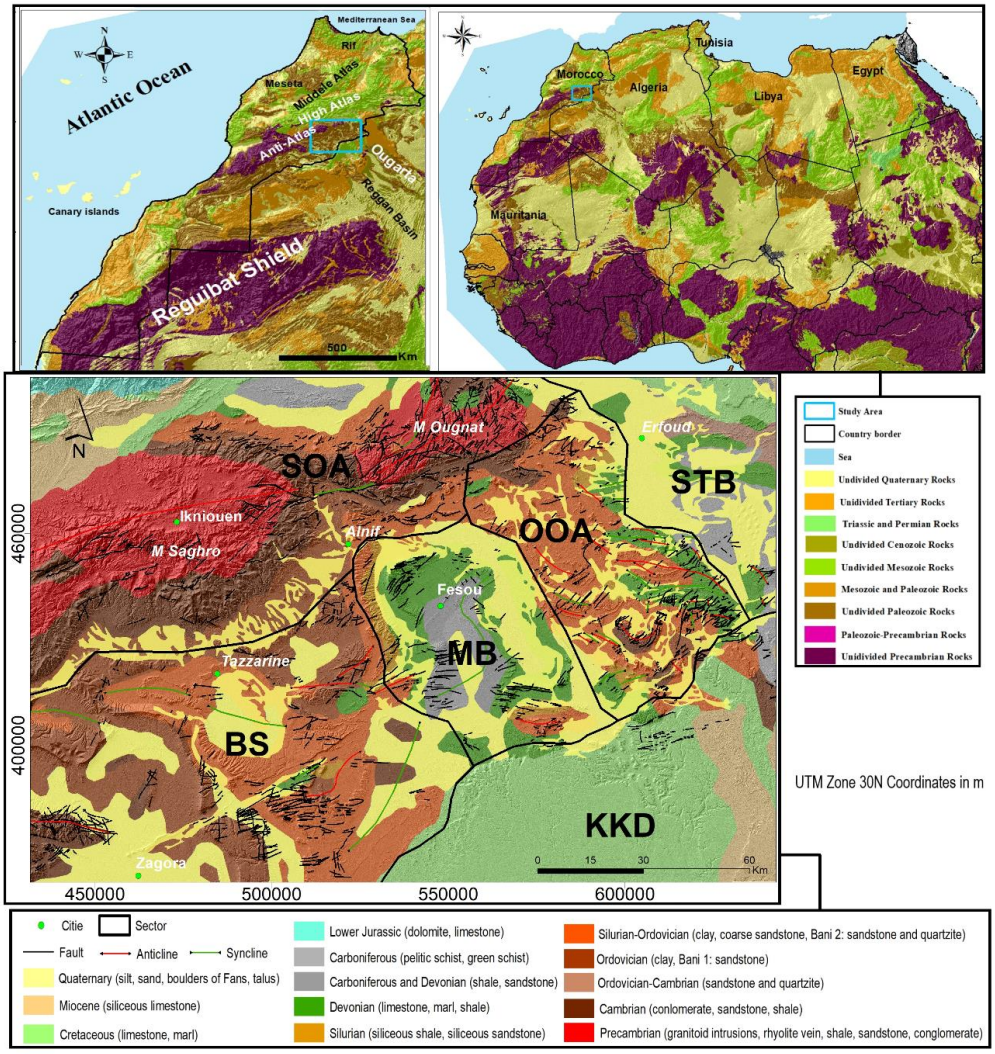

Fig. 1. Geological context of the studied area and location of the 6 geological sectors Modified from Baidder et al. (2016).

Table 1: Summary details of the 6 sectors

Sector	Area (Km²)	Mean Elevation (m)	Mean Slope (°)	Dominant lithology	Geomorphological Characteristics
BS	7810	882	7,9	Sandstone and quartzite, micaceous sandstone clay, green shale	First and second Bani ridge: monoclinal structures, Tazzarine basin
OOA	3527	780	7,7	Green sandstone and quartzite, green sandstone and volcanic rock lenses, quartzite sandstone, green shale siliceous sandstone, marl limestone, sandstone and pelite	shear zone that consists of a succession of anticlines and synclines
MB	3120	780	6,2	Sandstone and quartzite, schist, pelitic schist	basin structures and depressions, such as the Fezou syncline, lowland area at the foothills of the high reliefs forming part of a sedimentary basin
KKD	5048	743	6,5	Limestone, Marl, Siliceous limestone	Tabular sector of Cretaceous deposit
STB	2717	795	5,4	pelite, sandstone and quartzite, limestone, alluvial conglomerate, coarse sand, limestone cement conglomerate	lowland area, plains, mostly synclinal in character, anticlinal structures in the northern and southern part of the area
SOA	9255	1412	12,2	Amphibole granite, Rhyolite, Basalt, shale, sandstone, conglomerate, pink sandstone, green shale.	Precambrian basement that outcrops in two large inliers, extremely fractured by important tectonic structures.

This analysis was carried out on 230 basins extracted from 5 major endorheic basins, namely from the northeast to the southwest, the Ziz, Rhéris, Kem-kem, Maider and Draa basins. These endorheic basins and the procedure for the basins and channel network extraction from the ASTER-Global Digital Elevation Model are presented in Supplementary Material S1 and S2. The climate is arid in the north in both Saghro and Ougnat mountains, with annual rainfall of about 120 mm, and becomes extremely arid in the south, with only 50 mm per year (Hilali, 2015; Kassou, 2016).

2.2. Major parameters assigned to the basins:

For each of the extracted basin, the geographical coordinates of the barycenter were determined, as well as 16 parameters that reflect their topographic, geological and morphometric characteristics. These parameters were obtained through various remote sensing data (Landsat 8 OLI, Sentinel-1A and Sentinel-2A), a Digital Elevation Model (30 m resolution ASTER-GDEM), 5 geological maps of 1/200000 scale that cover the entire study area (Hinderleyer et al., 1977; Clariond et al., 1982; Destombes and Hollard, 1986; Du Dresnay et al., 1988; Choubert et al., 1989), and geological data of eastern Anti-Atlas from the United State Geological Survey (USGS, http://earthexplorer.usgs.gov/). The 16 parameters are detailed below.

2.2.1. Drainage network patterns parameter

The first is the type of drainage pattern identified in the extracted basins, with a code assigned to each pattern, as follows: 0 = dendritic, 1 = parallel, 2 = trellis, 3 = angular. The first step was to verify, for each basin, the adequacy between the extracted drainage network and the geological (scale 1/200000) and topographic (scale 1/100000) maps. Then the drainage pattern parameter was assigned on several criteria (general shape of the network, orientation, connection angles of tributaries, etc.) for recognition of drainage network patterns (Zernitz, 1932; Howard, 1967). In order to investigate the change in the drainage network orientation in the study area, the drainage network has been classified according to the associated rock type and structural regime. Five drainage network groups were identified, developed on the Precambrian bedrock, Paleozoic outcrops, Lower Mesozoic formations, Lower Neogene and those formed in Quaternary deposits.

2.2.2. Morphometric parameters

Morphometric characteristics for each drainage basin were calculated, namely the total area, the perimeter, as well as two shape indices known as the Gravilus compacity index (K_G) that reflects the stretched form of the catchments, and the Horton shape index (K_H), wish is indicative of the flood regime of the stream (Horton, 1932). K_G is defined as the ratio between the perimeter (P) of the basin to the perimeter of the circle having the same area (A):

$$K_G = \frac{P}{2\sqrt{\pi.A}} \quad (1)$$

K_H expresses the ratio of the basin area (A) to the length of the mainstream (L):

$$K_H = \frac{A}{L^2} \quad (2)$$

2.2.3. Topographic parameters

In order to identify which feature of the relief (Fig. 2a) best explains the hydrological behavior of the basins and the structure of the drainage network, 6 parameters were calculated. They are: 1 - MAX-Alt is the maximum elevation above the basin outlet, used to express the basin relief (Sangireddy et al., 2016). 2 - R1 is the relief ratio described by Melton (1957), and defined as the ratio of basin 'r' wish is the relief difference in altitude between the culminating point and the outlet, and the perimeter of the basin 'p'.

$$R1 = \frac{(ALTMax - ALTMin)}{P} = \frac{r}{p} \quad (3)$$

Where ALTMax is the altitude of the culminating point and ALTMin is the altitude of the outlet. 3 - R2 is the dimensionless Schumm relief ratio (Schumm, 1956; Melton, 1957; Rawat et al., 2013) defined as the ratio between the total relief of a basin 'r' and the longest dimension of the basin parallel to the principal drainage line 'L':

$$R2 = \frac{r}{L} \quad (4)$$

'L' is defined as the length of the equivalent rectangle:

$$L = \frac{K_G\sqrt{A}}{1{,}12}\left[1 + \sqrt{1 - \left(\frac{1{,}12}{K_G}\right)^2}\right] \quad (5)$$

The basin relief ratio (R1 and R2) indicates the general slope of a drainage basin and the intensity of erosion process occurring on the slope of the basin (Schumm, 1956; Asfaw and Workineh, 2019). 4 - The last topographic parameter is the Ruggedness number 'H' calculated as the product of drainage density 'D_d' and relief of basin 'r' both in the same units. It refers to the level of smoothness and roughness of the basin surface and its vulnerability for soil erosion. High ruggedness values indicate areas with uneven topography and sensitive to soil erosion (Strahler, 1954; Asfaw and Workineh, 2019).

$$H = r\ D_d \quad (6)$$

5 - 'Mean-slope' (Fig. 2b) denotes the average slope of each basin, and was calculated from the DEM by the slope tool available on the GIS software. The procedure calculates for each cell the maximum rate of variation of the altitude values with respect to its neighbors (Burrough and McDonnell, 1998). 6 - The Langbein concavity index (Langbein, 1964) was calculated as the ratio of the difference between ALTMax and H, the altitude at 50% distance between the source and the outlet, and the relief of a basin 'r'. The concavity index 'CI' indicates the channel steepness, the higher the value, the faster the channel gradient decreases.

$$CI = \frac{ALTMax - H}{r} \quad (7)$$

2.2.4. Drainage density parameter:

The drainage density is a key parameter that relates the operating geomorphological processes to the topography of a drainage basin (Sangireddy et al., 2016). It is expressed as the ratio of total channel length to total basin area (Km/Km²). After extracting the drainage density, the average drainage density 'MEAN-Ddrain' (Fig. 2c), which represents the average drainage density in each basin, was extracted using the 'Area

statistics' tool available on GIS software that calculates the values of the drainage density raster within each basin.

2.2.5. Geological parameters

The basin geological characteristics are represented by four parameters. First, the 'Structural control' parameter, which reflects the type of geological structuring that controls the drainage network and the basin geomorphology. Four types of structural controls were identified in the study area, by visual interpretation and image processing of satellite images, geological maps and other USGS data (van der Meer et al., 2014; Adiri et al., 2017; Fal et al., 2019; El Janati, 2019), but also from previous work (Robert-Charrue, 2006; Baidder et al., 2016). These four types of structural control are Tabular = 0, Folding = 1, Faulting = 2, and Faulting + folding = 3. The second parameter of the geological characteristics reflects the lithologic homogeneity or heterogeneity of the basin area. If a basin has a surface 80% covered by a lithological formation of the same lithological formation, it is described as homogeneous and it is assigned the code 0, otherwise, it is qualified as heterogeneous and it is assigned the code 1. The rock type parameter 'Rock-type' was based on a simplified basin lithology. For each basin, rock types were lumped into four major group, to which codes have been assigned: granitic-metasedimentary=3, volcanic=2, sedimentary=1, and quaternary sediment=0, broadly reflecting a change from harder to softer rock types.

The parameter "Lineament density" reflects the average density of geologic lineaments identified in each basin, expressed as the ratio of total lineaments length to total catchment area (Km/Km²) (Fig. 2d). The structural alignments identification was performed automatically by a computer algorithm based on the Hough transform method (Karnieli et al., 1996; Poncelet and Cornet, 2010; Aydogan, 2011; Renson et al., 2013; Bouramtane et al., 2017). The Hough transform algorithm was applied to the multi spectral image Landsat 8 OLI satellite (30 m resolution), the image of the Sentinel-2A satellite band 11 (10 m resolution) and the radar image Sentinel-1A band Intensity-VH. The 3 sets of geological lineaments obtained on the 3 images were merged while eliminating the duplicate or triplicate to avoid repetition of the information.

2.2.6. Location parameter

Finally, a location parameter was assigned by referring to the different sectors previously described, namely, Ougnat-Ouzina axis = 1, Kem Kem domain = 2, Banis sector = 3, Maider basin sector = 4, South-Tafilalt Basin sector = 5, and Saghro-Ougnat axis = 6.

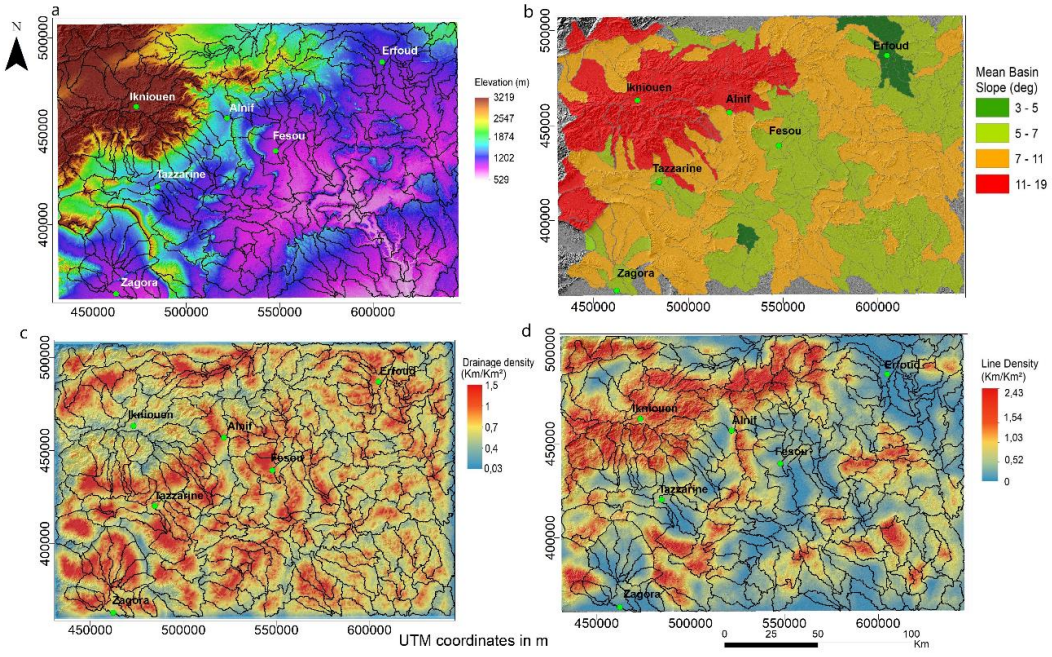

Fig. 2: Map of studied basin in the eastern Anti-Atlas, Green dots indicate locations of main cities, basins are outlined in bold: (a) Elevation (b) Mean basin Slope (c) drainage network mean density and (d) geological lineaments mean density.

2.3. Statistical tools

The dataset (230 basins x 16 parameters) was treated using multivariate statistical methods. A principal component analysis (PCA) was carried out by diagonalization of the correlation matrix in order to identify, quantify and rank the different sources of variability, and to explore the underlying phenomenon responsible for the drainage network variability. The procedure includes variables mean centering that sidestepped problems arising from the variable numerical ranges and units used by automatically autoscaling all variables to the mean zero and variance unit. When many parameters are available to characterize different groups of observations, it is not easy to characterize the degree of resemblance or dissimilarity between several groups, as 2D- or 3D-plots give only a partial vision of the information. Multivariate methods are essential, and among these techniques, linear discriminant analysis is a conventionally and widely used tool to study groups of observations that may have different characteristics. Linear discriminant analysis (LDA) is a generalization of Fisher's linear discriminant, a method used in statistics, pattern recognition and machine learning to find a linear combination of features that characterizes or separates two or more classes of objects or events. The resulting combination may be used as a linear classifier, or, more commonly, to reduce the dimensionality between before and after the classification. Agglomerative hierarchical clustering (AHC) is the most common type of hierarchical clustering used to group objects in clusters based on their similarity. It is also known as AGNES (Agglomerative Nesting). The algorithm starts by treating each object as a singleton cluster. Next, pairs of clusters are successively merged until all clusters have been merged into one big cluster containing all objects. The result is a tree-based representation of the objects, named a dendrogram.

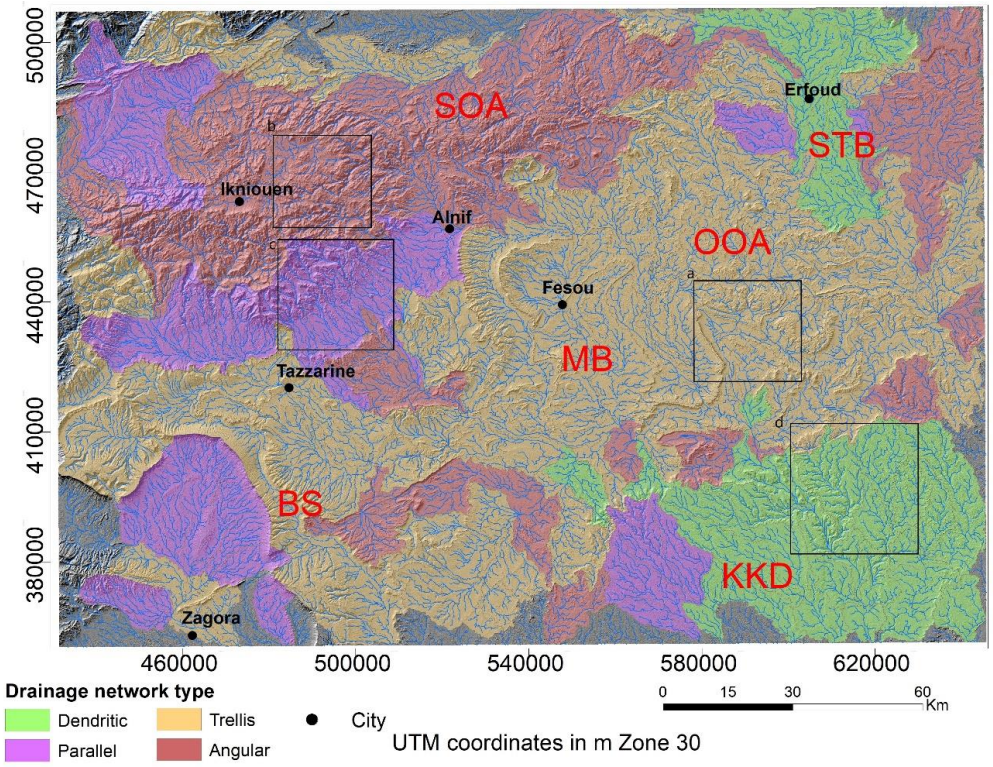

Figure 3: Distribution of the different drainage network patterns in the Eastern Anti-Atlas. (See figure 4 for black boxes a, b, c and d)

3. RESULTS

Drainage network distribution:

A total of 230 basins with area ranging from 9.5 Km² to 482 Km² were extracted. The drainage network patterns were identified as follows (Fig. 3). One hundred and six basins showed trellis drainage patterns developing mainly on the Paleozoic folded cover. Fifty basins had angular patterns and developed on the ancient Precambrian formations in both Saghro and Ougnat inliers, and in the extreme northwest on the Erfoud anticlinorium. Forty five basins were identified as dendritic patterns in the Ziz alluvial plain to the northwest, and in the southwestern extent of the Kem-Kem domain. Finally, twenty nine basins had parallel

patterns observed on the southern and western flanks of the Saghro and Ougnat inliers respectively and on the Feija escarpment north of the city of Zagora and the western part of Kem-kem domain. Selected examples are shown in (Fig. 4).

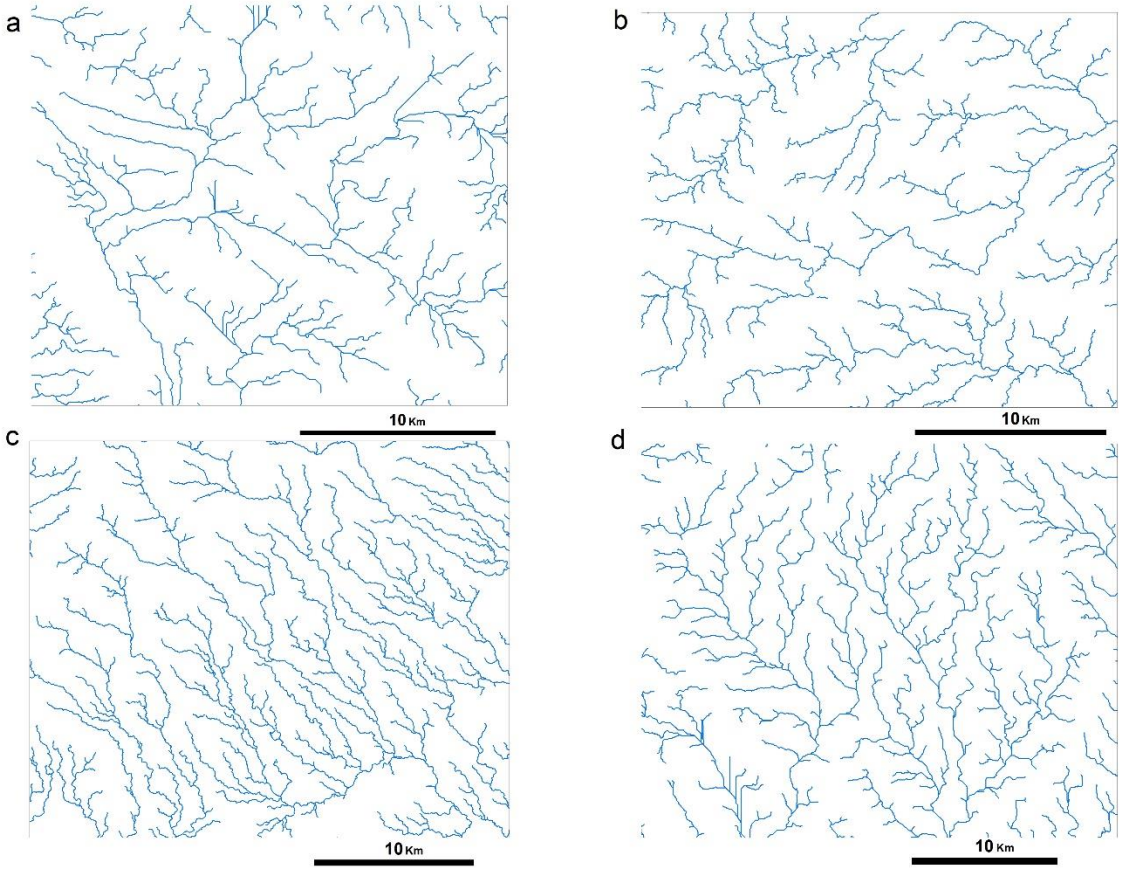

Fig. 4: Example of identified drainage network patterns: a= trellis, b= angular, c= parallel, d= dendritic (see location as black rectangle in Fig. 3)

Statistical distribution parameter per parameter:

The relationships between some parameters taken 2 to 2 are presented in Fig. 5 that shows, for example, that the relief ratio 'R1' increases with the ruggedness number 'H' on all basin types, and that the scatter plots overlap widely. The parallel-type networks are slightly individualized (Fig. 5a and c), but their superposition with angular and lattice types networks does not allow them to be separated into an isolated group, as shown in the means and standard deviations cross plot (Fig. 5c). The same is true, for example, for the 'Lineament Density' and 'Mean Slope' parameters (Fig. 5b and d). This approach is therefore unsuccessful for the discrimination of types of drainage networks, hence the use of multivariate methods.

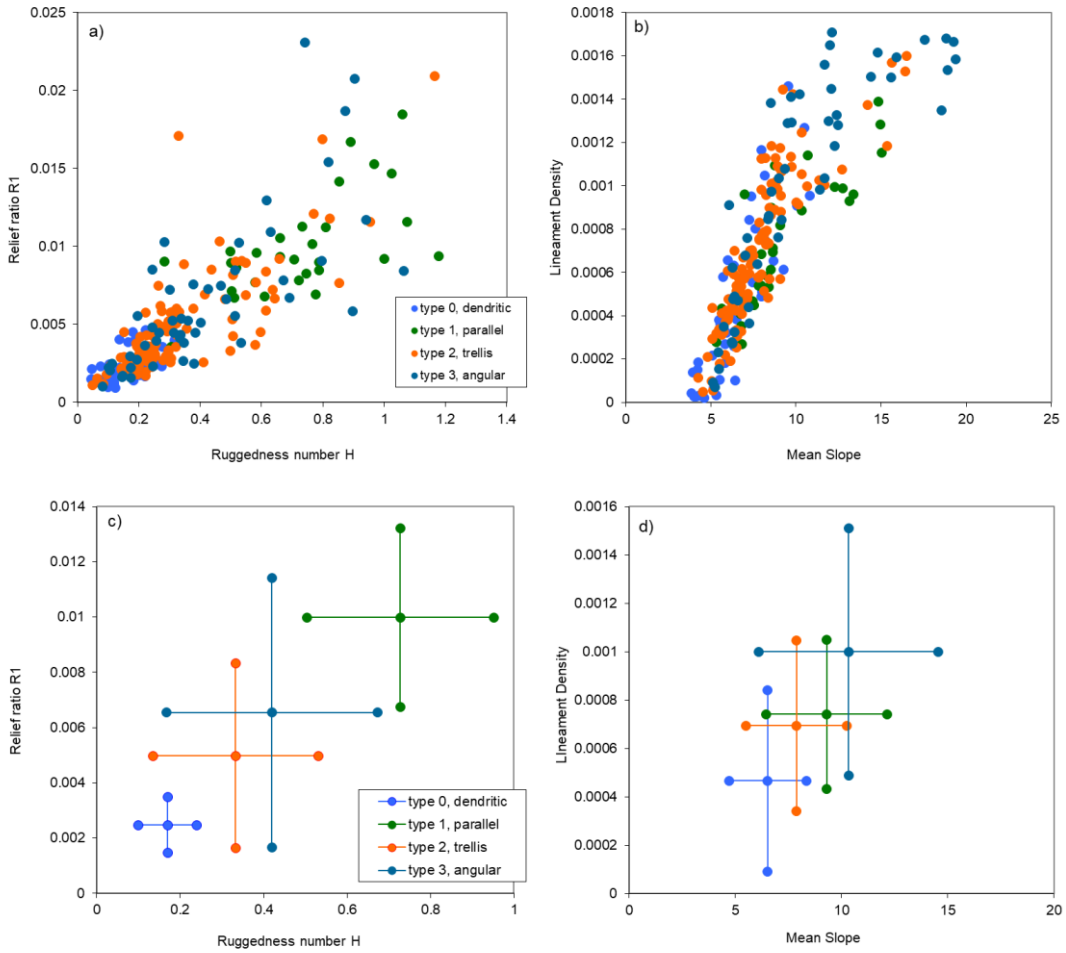

Fig. 5: a) and b) : Distribution plot for the parameters Rudgeness number 'H' and Relief ratio 'R1', and Mean-Slope and Lineament Density, respectively, for the 230 extracted basins and depending on the type of drainage network. c) and d) Mean values and standard deviations for the same parameters.

Principal component analysis:

The results of the PCA are presented in Fig. 6 and Table 2. The variance distribution according to the Principal Components (PCs) showed that the information was distributed in many PCs, indicating complex and non-redundant information. The first five PCs showed eigenvalues higher than unity indicating that they convey more information than a single variable. The first four PCs accounted for 72% of the total variance of the dataset. The first PC (PC_1), which explains 35.5% of the total variance, essentially represented topographic parameters (H, R1, R2 and ALT-MAX), slope parameters (Mean-slope) as well as the parameter lineament density. Although less marked, the parameters related to the basin shape K_H, the Homogeneity, the area, structural control and the type of drainage patterns were positively correlated to this PC_1. The second PC, PC_2, accounted for 14.4%, involving a group of morphometric parameters (Surface, Perimeter, K_G) and to a lesser extent a second group of parameters related to type of drainage network, and the geological parameters structural control and Homogeneity. The type of drainage pattern was clearly correlated with the third PC (PC3, 12.7% of the variance) as well as the geological parameters (structural control and homogeneity) reflecting a close relationship between the type of drainage network and the geological parameters. This relationship seemed to be stronger for small and medium size basins as suggested by the negative correlation with the morphometric parameters (Surface, Perimetre and Concavity). Finally, the fourth PC (PC_4, 9.3%) was correlated with the drainage density, secondarily with the morphometric parameter K_G, the Area and the Ruggedness number H.

Thus, the variance distribution showed a complex pattern, but the type of drainage pattern appeared on the first three PCs with strong correlation with topographic and geological parameters. For the latter, the contribution of the structural control and homogeneity played a major role.

Table 2: Principal Components, respective eigenvalues and contribution to the total variance.

	PC_1	PC_2	PC_3	PC_4	PC_5	PC_6
Eigenvalues	6.04	2.45	2.16	1.59	1.35	0.94
Contribution (%)	35.53	14.42	12.69	9.34	7.96	5.50
Cumulated contribution (%)	35.53	49.94	62.63	71.97	79.93	85.44

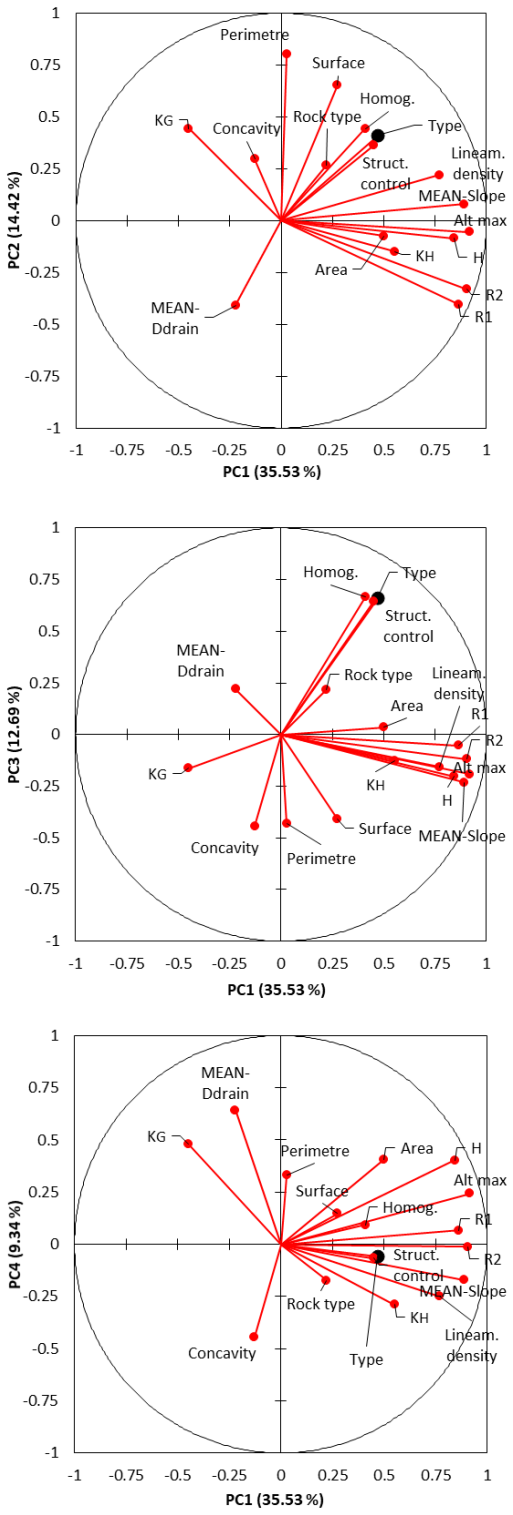

Fig. 6: Distribution of the variable "type of drainage pattern" together with the other 16 parameters in the score plots PC_1-PC_2, PC_1-PC_3, and PC_1-PC_4

Linear discriminant analysis:

The linear discriminant analysis identified three functions that properly distinguish 90% of the basins according to the type of drainage pattern. The first function F_1 alone identified 69.2%, whereas F_2 and F_3 function distinguished 24.2% and 6.6%, respectively (Fig. 7). The confusion matrix (Table 3) represents the degree of accuracy of basin discrimination as a function of the type of drainage pattern. The dendritic patterns were distinguished with a success rate of 100%. Parallel patterns also showed a high discrimination accuracy 93.1% with only 2 badly discriminated basins among 29. Trellis and angular patterns appeared

distinct from the other patterns with a lower discrimination value, although still at 88.7% and 82% respectively, i.e. 12 badly discriminated basins among 106 for trellis patterns and 9 badly discriminated basins among 50 for angular patterns.

Table 3: Confusion matrix of the Linear Discriminant Analysis

from \ To	0	1	2	3	Total	% correct
0	45	0	0	0	45	100%
1	0	27	0	2	29	93.1%
2	0	0	94	12	106	88.7%
3	0	1	8	41	50	82%
Total	45	28	102	55	230	90%

Table 4 shows the correlation values between the different parameters and the three discriminating functions. The first discriminant function (F_1, 69.18%) relied mainly on the geological characteristics, and presented high correlation values for the parameters "structural control" and "homogeneity" (0.844, 0.933 respectively). The second discriminant function (F_2, 24.20%) have a strong negative correlation with topographic parameters H, R1, R2 and ALT-MAX (-0.737, -0.588, -0.481 and -0.502, respectively) and with a less extend the drainage density parameter (Mean-Ddrain, -0.426). The third discriminant function (F_3, 6.62%) relied mainly on the geological parameter "Area" with a correlation of 0.657, secondarily on the parameter that describe the basin mean slope (Mean-Slope, 0.576), and on the geological parameter "lineaments density" with a correlation of 0.515. Full equations of the discriminant functions are given in supplementary material S3.

Table 4: Correlations between variables and discriminant functions (higher values are in bold)

	F1 (69.2%)	F2 (24.2%)	F3 (6.6%)
H	0.288	**-0.737**	0.267
R1	0.294	**-0.588**	0.293
R2	0.299	**-0.481**	0.250
Alt max	0.343	**-0.502**	0.379
Concavity	-0.326	0.354	0.357
Area	0.222	-0.281	**0.657**
Structural control	**0.844**	-0.007	0.147
Homogeneity	**0.933**	0.027	-0.033
Rock type	0.284	0.181	0.056
Surface	0.112	0.053	0.010
Perimetre	-0.005	0.089	0.114
K_G	-0.231	0.120	0.154
K_H	0.196	-0.097	-0.098
MEAN-Ddrain	-0.053	**-0.426**	-0.257
MEAN-Slope	0.302	-0.176	**0.576**
Lineaments density	0.344	-0.045	**0.515**

F_1 discriminated very well the dendritic from the parallel pattern and from the group trellis + angular pattern. F_2 separated the parallel pattern from the other patterns. Although F_3 carried the least variance, it was the only function to separate trellis from angular patterns. The F_1-F_2 score plot (Fig. 7) displays each group with an accuracy rate of 93.6%. The discriminant function F_1 separates the basins controlled by the geological factors with the structural control and homogeneity parameters, i.e. the angular and trellis patterns, from the basins not controlled by this factor, i.e. the dendritic and the parallels. The centroids of angular and trellis patterns have positive coordinates along F1 axis, whereas those of dendritic and parallel pattern are negative and close to zero, respectively (Fig. 7). F_2 separates the basins that are influenced by a high topography and high relief ratio, as is the case with the parallel pattern, from the basins that are weakly influenced by this factor, for example the dendritic pattern, or those not controlled by this factor, such as trellis and angular patterns (Zernitz, 1932).

The F_1-F_3 plot (Fig. 7), allowed a discrimination of 75.80%, and separated the basins, on the one hand according to parameters of geological structuring (Structural control on the F_1 axis) and on the other hand according to their locations in the different sectors (Area parameter on the F_3 axis). The centroids of dendritic and parallel patterns, not affected by the geological structure of each sector neither by the drainage or lineament density, show coordinates towards zero values along F_3. The parallel pattern, not influenced by the geological structuring, also had values close to zero on F_1, i.e., it centroid was in the center of the F_1-F_3 plot. As in F_1-F_2 plot, the dendritic patterns show negative coordinate along F_1 since they have negative correlations with geological parameters. In other words, the absence of geological factors in a basin contributes to the formation of dendritic patterns. F_3 separates the trellis and angular patterns with centroids converging towards negative and positive values along F_3, respectively.

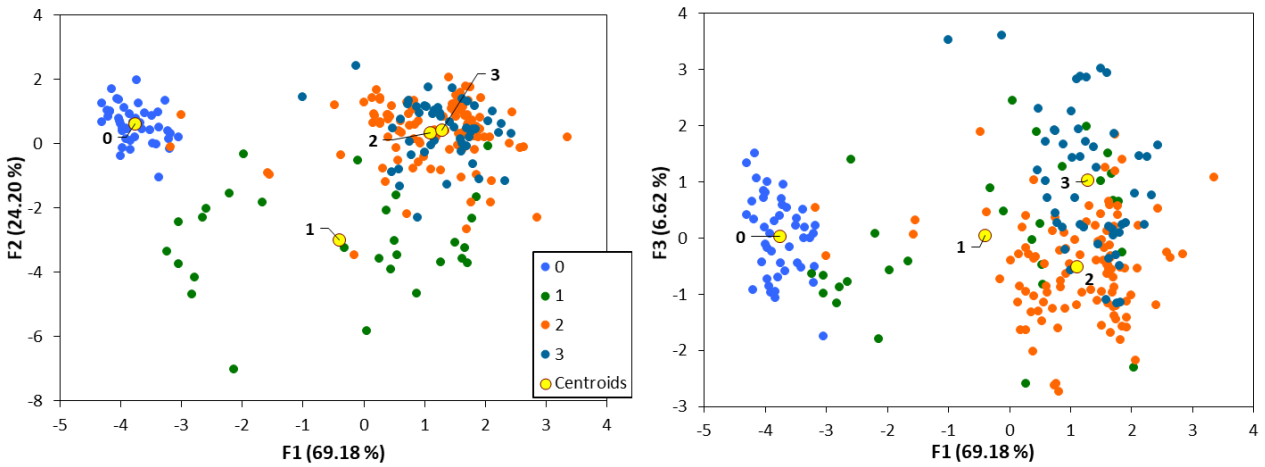

Fig. 7: Distribution of the observations and centroids of each type of drainage network pattern in F_1-F_2 and F_1-F_3 score plots (0 = Dendritic, 1 = Parallel, 2 = Trellis, 3 = Angular).

Agglomerative Hierarchical Clustering:

PCs are a linear combination of the 16 variables, i.e. macro-parameters that can be used for classification. The first seven PCs accounted for about 90% of the variance of the dataset. The results of the agglomerative hierarchical clustering based on the coordinates of the centroids throughout the axes of the first seven PCs are presented in Figure 8. This made it possible to specify the degree of similarity or dissimilarity between the different types of drainage network patterns. Clearly, the dendritic pattern was individualized from the other patterns, whereas the trellis and angular patterns showed higher similarity, forming an isolated group. The parallel pattern was halfway between the group angular + trellis and the dendritic patterns.

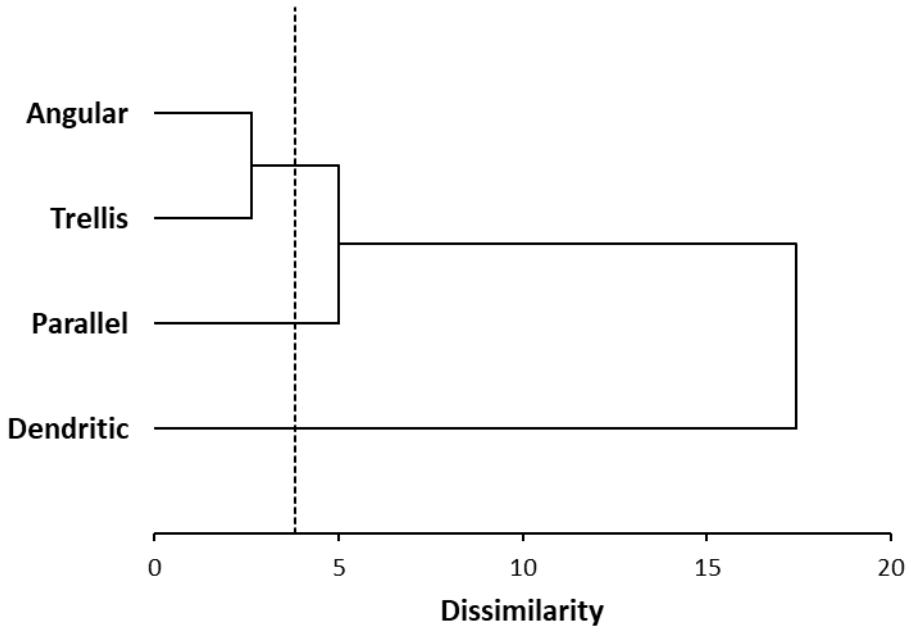

Fig. 8: Dendrogram obtained from agglomerative hierarchical cluster analysis on drainage patterns centroids based on the first seven principal components.

Fig. 9 show the principal and secondary orientation of the hydrographic network developed on each geological age, from Precambrian to Quaternary, analyzed individually using frequency and length weighted diagrams. The main flow directions, NE-SW, NW-SE and E-W are observed for all ages, but with a higher order over Precambrian and Palaeozoic formations. The NW-SE orientation becomes predominant over the Lower Mesozoic and Lower Neogene formations.

4. DISCUSSION

Trellis and angular drainage patterns are widespread in the eastern Anti-Atlas, suggesting that hydrological processes in this region are subject to structural control (Howard, 1967; Stokes et al., 2008; Pereira-Claren et al., 2019). The first 3 principal components highlight the parameters that describe the topography, slope and geological parameters (Structural control, Area, Homogeneity and Lineaments density), all positively correlated with the type of drainage pattern. These results are in agreement with the work of Zernitz (1932), Howard (1967) and Twidale (2004), as the factors that explain the most variance between the different types of drainage pattern are those that reflect the topography and geological structuring (Stokes et al., 2008; Pereira-Claren et al., 2019).

Principal components furnish macro parameters, i.e. synthetic data that convey strong and significant information and, therefore, are particularly suitable for digital mapping and spatial analysis (Rezende-Filho et al., 2015). The distribution of PCs values is showed in Fig. 10. The Highest values of PC_1 denote the influence of a high relief with steep slope, heterogeneous rock lithology and high intensity of fracturing and geological deformation. Higher PC_1 values are observed in the SOA sector, on the one hand, at the heart of the Neoproterozoic inliers where angular drainage patterns occur, and on the other hand on the northern and southern flanks of the Saghro inlier, where strong slope gradient are associated with parallel patterns. Moderate values along PC_1 are found in the MB, OOA and BS sectors, where almost parallel or slightly arcuate outcrops exert structural control on the drainage pattern and reduce the influence of slope parameter. This led to the formation of trellis patterns associated with the Bani structures in the BS and MB sectors, and with anticlinal and synclinal flanks in folded sedimentary sequences in the OOA sector. Low and negative values along PC_1 reflect low relief, a relatively gentle slope and a lithology characterized by Cretaceous and Quaternary sedimentary deposits, and a lack of prominent geologic and tectonic structures. They are observed in the KKD and STB sectors, reflecting the weak influence of the slope factor and the presence of dendritic models. The vast alluvial zones of these areas strongly influence this phenomenon. The observation of some parallel network in the western KKD sector indicates a slight change in slope gradient from east to

west. Jung et al. (2011) observed a similar phenomenon and calculated that the drainage networks present a transition from dendritic to parallel from an increase of 1% to 3% of initial regional slope.

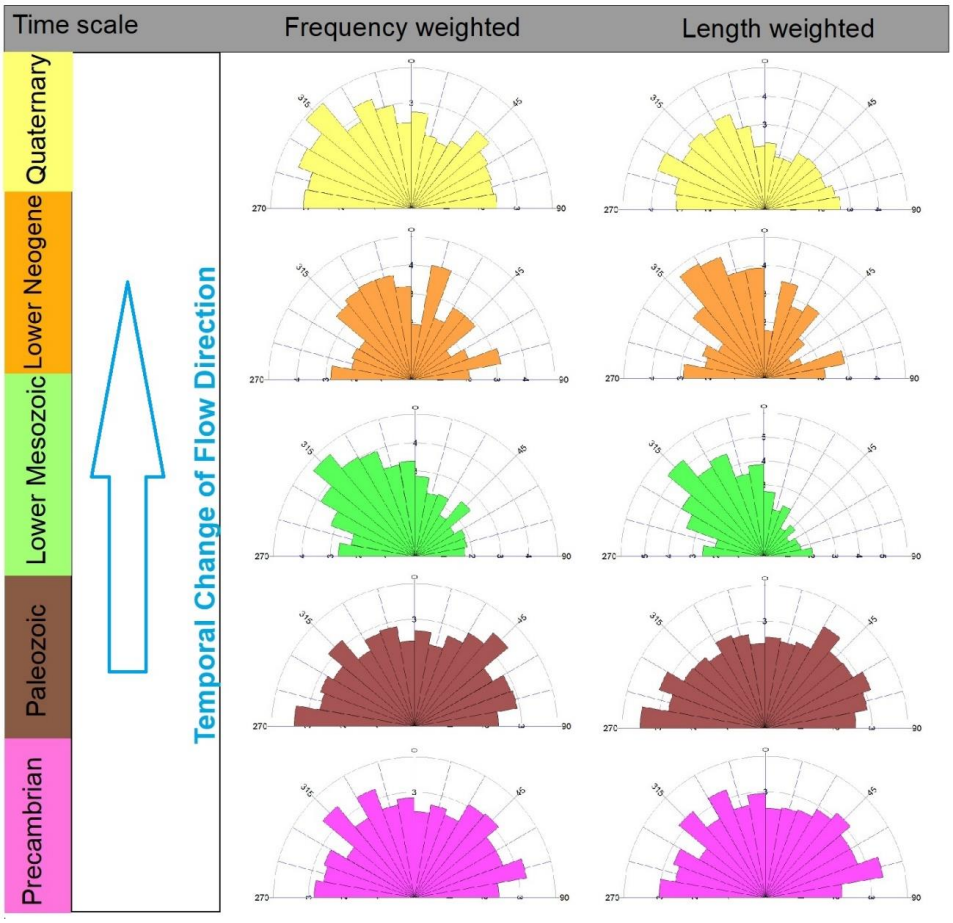

Fig. 9: Change in the azimuth direction of the drainage network in the Eastern Anti-Atlas from Precambrian to Quaternary formations.

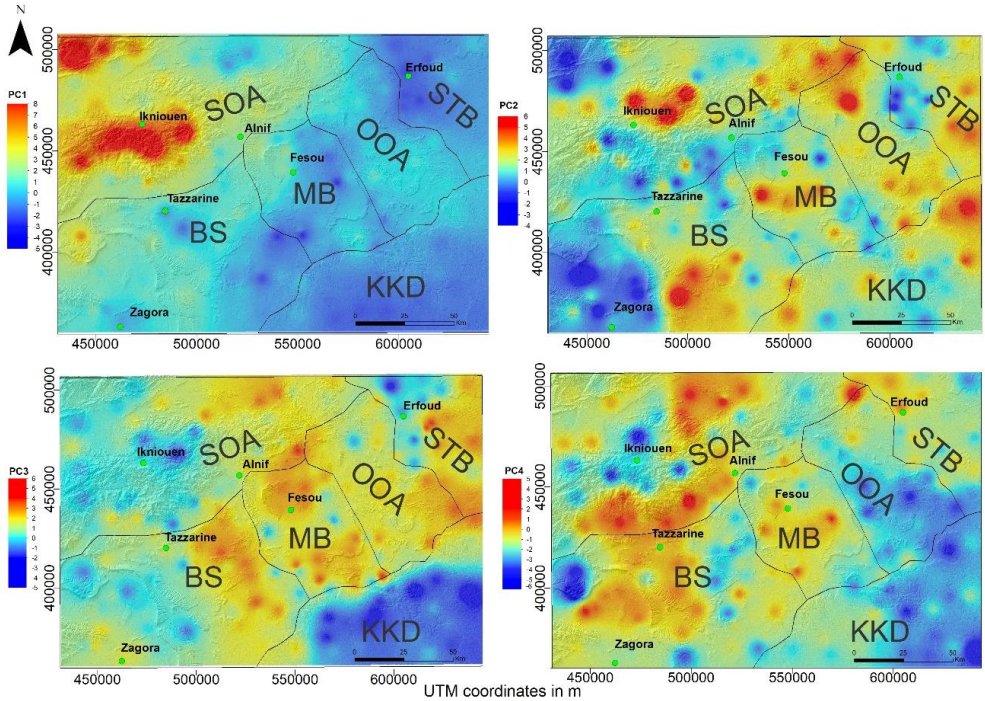

Fig. 10: Distribution of the main PCs (PC_1 to PC_4) on the studied area.

PC_2 is also associated with the type of drainage network. It is positively correlated with morphometric parameters (Surface, perimeter and K_G) and geological parameters (Structural Control and Homogeneity) and negatively correlated with drainage density. These characteristics depend mainly on the size and shape of the basin, the lithology and the extent of the drainage network (Horton, 1942; Melton, 1957). High PC_2 values (> 4) are observed at northeastern and western part of the KDD sector, in the northwestern and southwestern parts of the Erfoud region, east of Iknioun, and on the Bani structures in the east - northeast of Zagora (Fig. 10), where most of the basins are large and elongated. Negative values on PC_2, which reflect a dependence on drainage density, were identified in the south and north flanks of the SOA sector and in the southwestern part of the BS sector. In these areas, steep slopes on clay, shale and sandstone rocks result in higher drainage density (Melton, 1957). In the STB sector south of Erfoud, the negative values correspond to the alluvial plain, where the absence of geological structuring and low slope lead to high drainage densities.

PC_3 highlights the relationship between the geological parameters and the type of drainage pattern. These parameters collectively reflect the influence of the geological structuring on the control of drainage network for the basins with the angular and trellis pattern. In other words, the basins with a high coordinate in PC_3 are likely to reflect the presence of one of these two types of drainage patterns. The high positive PC_3 values are observed in the MB, OOA, and in the east of BS, SOA and STB sectors, where both trellis and angular patterns prevail on small to medium size basins with relatively heterogeneous lithology, over folded and fractured terrain (Fig. 10). Negative values in PC_3 reveal a dependence on topographical characteristics, in particular altitude variation, and basin size. Such negative values occur in KKD and east STB sectors in wide basins with gentle slope and mainly dendritic networks, on Cretaceous deposits in the first and alluvial plains in STB sector, attesting for the weak influence of structural control on the drainage network. Generally large basins with branching networks like apple trees indicate a lack of control structure or slope over the drainage pattern, which is observed in the dendritic pattern (Zernitz, 1932). The low PC_3 values (between 2 and 0) in the western part of SOA sector is related to the high variation in altitude from the center of the Saghro inlier towards its northern flank. In this region, hybrid drainage patterns occur, from angular networks in wide basins upstream, following major faults, to parallel networks with narrow basins downstream in the flank of the inlier. Zernitz (1932) observed the same behavior in northwestern Finland, where some rivers run parallel to fault zones. These faults are structural and often accompanied by conjugated fractures, leading an angular configuration of the drainage network.

Finally, high PC_4 values occur in areas that presents a combination of high drainage density and the presence of sedimentary deposits, which is particularly clear in the southern flank of the SOA sector and the northern part of the Zagora region. Together, the results highlighted by PC_2 and PC_4 are consistent with observations made by Day (1980), Mueller and Pitlick (2013) and Sangireddy et al. (2016), as sedimentary rocks show relatively high values of drainage density compared with granitic, volcanic, and meta-sedimentary rocks.

The three discriminant functions Identified from the Linear Discriminant Analysis show that the basins can be distinguished with a high rate (90%) from their type of drainage pattern, using geologic, topographic and morphometric parameters. The confusing patterns mainly involve trellis and angular patterns and are false positive classifications. Indeed 12 trellis patterns were discriminated as angular and 8 angular patterns were discriminated as trellis. In the same way F_1, strongly correlated with the parameters that describe the geological structuring, groups the trellis and angular patterns in a same set and distinguishes them from the dendritic and parallel patterns, characterized by the absence of geological structuring. Both analyses, PCA and LDA, provide consistent results, especially PC_3 and F_1, given the close relationship between trellis and angular patterns, and the similar geological and geomorphological conditions for their formation. These conditions are folded sedimentary branching, converging, diverging or roughly parallel faults and joints and/or faults at right angles, which are generated by similar geological structuring factors (Zernitz, 1932; Howard, 1967; Twidale, 2004).

Finally angular and trellis patterns were separated by F_3, because of the high weight of the Area parameter, representing the geological sector of the basin's location. The distinct geology and geomorphology of each sector play a major role in determining the type of drainage systems, particularly those heavily influenced by geological structuring. Angular pattern basins are mainly located in the Saghro-Ougnat sector, i.e. areas composed of Proterozoic and Paleozoic terrains with high fracturing densities. This area was strongly impacted by several phases, mainly during the Neoproterozoic Panafrican and the late Paleozoic Hercynian

orogenies remobilizations (Hefferan et al., 2014). Many of the inherited faults were reactivated during the Alpine collision and High Atlas inversion, this last event did not cause any direct deformation in the Eastern Anti-Atlas, except a general uplift combined with the effect of a recent thermal anomaly, these inherited faults still constituting weak features (Robert-Charrue, 2006, Frizon de Lamotte et al., 2008; Soulaimani et al., 2014; Gouiza et al., 2017). Among these faults in SOA sector, Bou laghzazil-Tinifift, Tizi n'boujou and Arekouz fault (Fig.11a and b) are the main ones controlling a drainage network that follow the orientation of faults corridors, drawing angular shapes. Our finding are consistent with the conclusions of Zernitz (1932), as angular drainage networks occur in area with prominent structural control, and the pattern is directly conditioned by the right-angled jointing or faulting of rocks (Stokes et al., 2008; Burr et al., 2013; Pereira-Claren et al., 2019).

On the other hand, trellis pattern networks are mainly found in the Bani (BS), Maider basin (MB) and Ougnat-Ouzina axis (OOA) sector (Fig. 11d-c), i.e., in areas with a high deformation of geological structures and the presence of huge folded outcrops. Trellis patterns occur around and on the flanks of the prominent folds in the OOA sector, some with spectacular shape consisting in large crescent- or boomerang-shaped Cambrian structures, easily observed on satellite images. They are the Jbel Tijekht, Jbel Tadout and Shayeb Arass anticlines, as well as Ottara and Amesseoui synclines. Baidder et al. (2016) reported that these large Cambrian crescent-shaped or boomerang structures reflect inversion tectonics, describing locally a double fold mechanism controlled by faults that lead to basement exposure.

Similarities and classification confusion between angular and trellis patterns has been observed by other authors. Based on the deviations of drainage patterns from self-similarity, Mejía and Niemann (2008) observed that the shape characteristics of dendritic networks are self-similar at different scales of observation. The shape characteristics of parallel networks are self-affine, presenting an invariant image by anisotropic transformation and both angular and trellis networks are approximately self-similar. More recently, Jung et al. (2019) used a classification method based on quantitative parameters, namely the tributary junction angles, discriminate 5 drainage network patterns classes, dendritic, parallel, pinnate, trellis and rectangular. Their proposed method clearly discriminated dendritic, parallel, and pinnate networks, but differences between angular and trellis network types were hardly distinguished.

In the Banis sector, the trellis patterns occur in a geomorphological context that consists of alternating cuestas and deep depressions, typical of the EAA. These cuestas consist of sandstone ridges of the first and second Bani of Ordovician-Silurian age. The drainage networks flow in a straight line along to the greatest slope on the backs of the Cuestas towards the Feijas depressions. Then, the drainage networks adopt their layout and their orientation, which gives a characteristic trellis shape, controlled by the edges of the outcrops of formations, whose resistance varies in the parallel belts (Zernitz, 1932) (Fig. 11d).

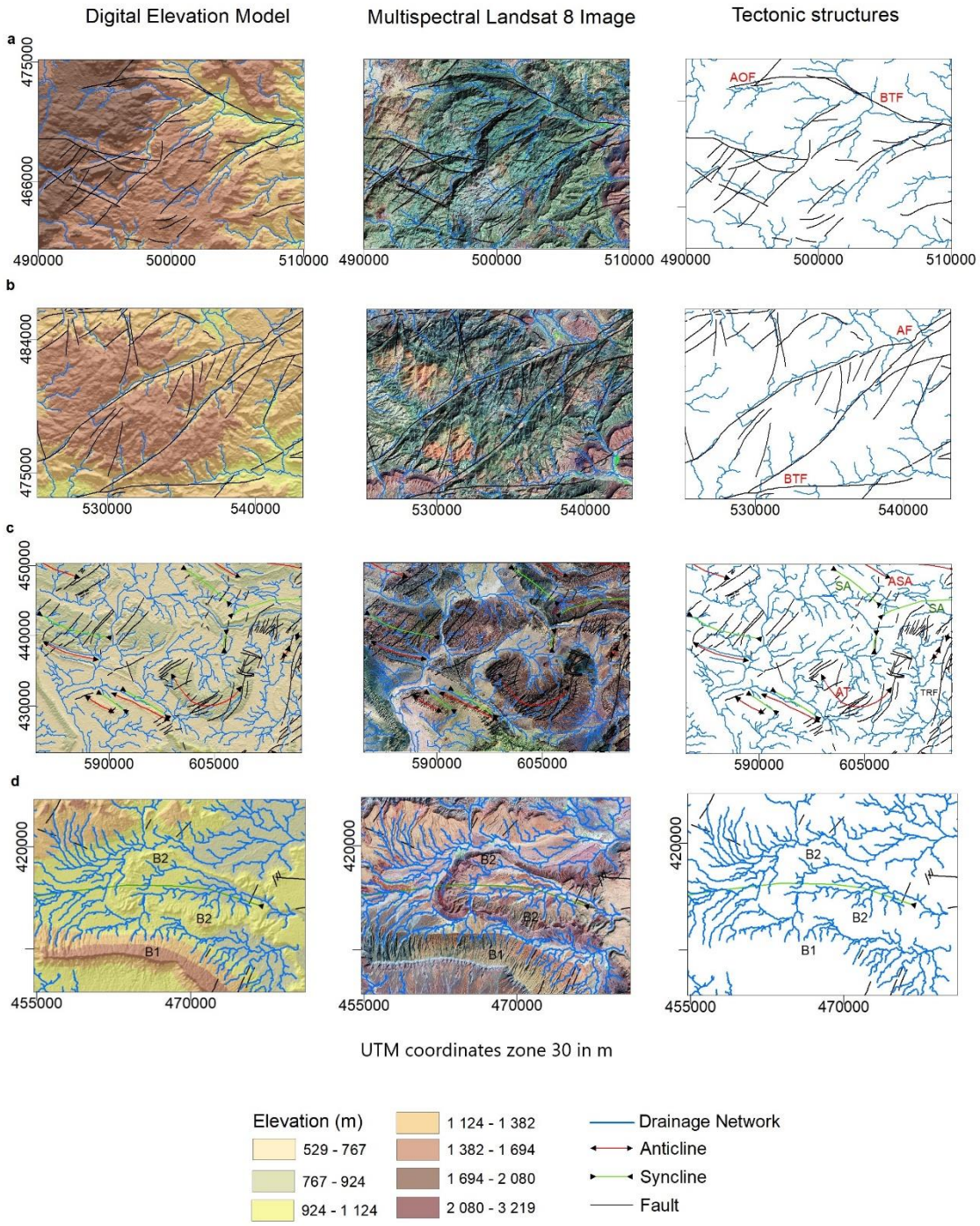

Fig. 11: Examples of relationship between major structural features (faults, synclines, anticlines) and drainage networks in (a and b) the Saghro-Ougna axis sector, (c) the Ougnat-Ouzina axis sector, and (d) the Bani sector. AOF = Assif n'Oussif Fault; BTF = Boulghzazil-Tinifift Fault; AF = Akrouz Fault; TRF = Tizi n'Ressas Fault; ASA = Anticline of Shayeb Arras; SA = Syncline of Amessoui ; AT = Anticline of Tijekht; B1 and B2 = Sandstone first and second Banis. (See the locations of the maps in Supplementary Material S4)

Parallel pattern basins are individualized by the F_2 discriminant function, which is mainly based on topographic parameters (H, R1, R2 and ALT-MAX). The result is consistent with the idea that the topography is the determining factor of this type of drainage pattern, which is generally associated with steeply to moderate sloping regions (Zernitz, 1932; Howard, 1967; Twidale, 2004; Radaideh et al., 2016). In the study area, parallel pattern basins with relatively high relief values (Fig. 2a) are located in the northwest, on the southern edge of the Saghro inlier, and to the southwest on the escarpment of the Feijas, and northeast of

the city of Zagora (Fig. 12a and b). They are also found west of the KKD sector, with higher maximum altitude and slope gradient (Fig. 2a and b). In addition, the parameters that reflect the drainage density (MEAN-Ddrain) have high coordinate values in F_2. This suggests the existence of a process that, in addition to the control by the slope, incorporates the drainage density. This observation is consistent with Johnson (1932), who suspected a relationship between slope and drainage density: the steeper the slope, the more parallel patterns are developed, and the more the drainage density increases (Twidale, 2004), as it appears in Figure 11 (a and b). The discriminant function F_2 makes it possible to distinguish basins as a function, on the one hand, of the influence of the slope on their drainage networks and, on the other hand, of the drainage density. Thus, F_2 makes it possible to separate the parallel pattern basins controlled by high relief and a steep slope gradient, the dendritic pattern basins characterized by a low slope gradient, and finally the trellis and angular pattern basins, mainly controlled by the geological structuring.

A few confusions in the parallel patterns were made using discriminant functions, with two parallel patterns identified as trellis, and one angular as parallel. In the SOA sector, angular networks are observed within the inliers in a strongly fractured area, and they connect to parallel networks developed on the strongly inclined Palaeozoic cover in the southern edge of the inliers. Such organization of the drainage networks may reflect a structural control by the formation of the Inliers. The relationship between angular and parallel in region where structural control occur has already been described by Zernitz (1932) that observed rivers running along parallel fault in north-western Finland. These faults, structural and most commonly accompanied by conjugate fractures, lead to angular network pattern. In the Bani sector, parallel and trellis networks developed on the same folded Palaeozoic formations, however they differ in their degree of parallelism resulting from a progressive steepening of slope, in relation with the degree of resistivity to erosion (Fig. 11d and 11b) (Howard, 1967). In the OOA sector, trellis drainage networks are restricted to a parallel relationship between tributaries (Fig. 11c). In the simple parallel model, parallelism may occur between tributaries or unrelated streams (Fig. 12a and b) (Zernitz, 1932). As revealed by PC3, in the Bani sector, because of alternation between ridges of hard sandstone (first and second Bani) and clay levels (Feija and Ktaoua shales) trellis networks have developed, although restricted to a parallel relationship between secondary tributaries, which are usually elongated and connect downstream at right angles (Zernitz, 1932) (Fig. 11c). In addition, parallel models have developed north of Zagora on the escarpment of the first Bani, flowing southwards over the gently inclined clay deposits. Because of uniform resistivity to erosion, the drainage network show a parallelism between all tributaries as well as between unrelated channels (Fig. 12b).

The separation of the dendritic patterns from others patterns in the two-dimensional space F1-F2 reflects a specificity of this drainage pattern. The positioning of the centroid with a positive but close to zero coordinate on F_2, and clearly negative on F_1 reflects the control by a low slope gradient and the absence of control by geological structuring. Of course, dendritic-pattern basins were not expected to have high F_1 values, because these drainage patterns are formed in areas without significant structural control, a lack of geomorphologic structures, a homogeneous lithology, and a slope gradient from weak to zero (Zernitz, 1932; Howard, 1967). These characteristics generate dendritic patterns characterized by irregular branching in all directions with the tributaries joining the main stream at any angles. These findings are observed in the EAA, where the dendritic patterns are exclusively in tectonically stable zones, with low relief and homogeneous lithology, as the case of the Kem-kem domain, consisting exclusively of Cretaceous deposits, and within the sedimentary basin of South-Tafilalat with flat lying Quaternary sediments (silt, sand, alluvial fans and talus) (Fig. 12c and d). Due to lack of marked structural control, and homogeneous lithology in these areas, the drainage network consists of channels oriented in a wide range of directions, leading to high drainage density.

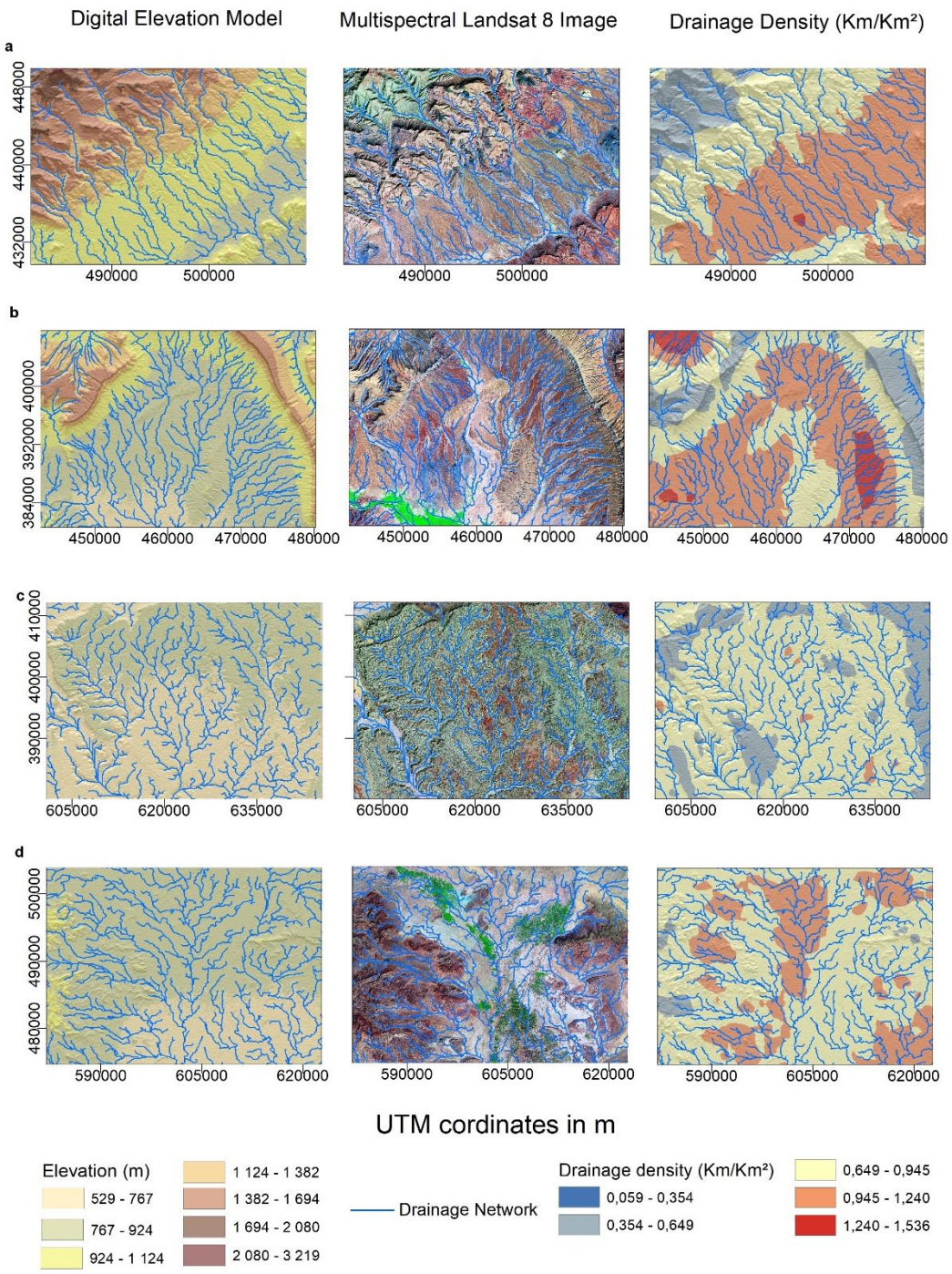

Fig. 12: Examples of relationship between parallel and dendritic drainage patterns, and slope gradient, geological structures and drainage density. (a) Parallel drainage patterns on the western edge of Saghro inlier in Saghro-Ougnat axis; (b) Parallel drainage network north of Zagora city in the Feija escarpment (BS Sector). (c) Dendritic drainage patterns in the Kem-Kem Domain, (d) Dendritic drainage patterns in the South-Tafilalt basin. (See the locations of the maps in Supplementary Material S4)

The results of the Agglomerative Hierarchical Clustering analysis are in agreement with the results of the LDA with respect to, on the one hand, the confusion between the parallel, trellis and angular patterns, due to similar factors responsible for their formation, and on the other hand, the individualization of a dendritic pattern. The position of the parallel type in the dendrogram between the angular+trellis group and the dendritic patterns could not be only due to its formation conditions, but could also stem from transition phenomenon from one drainage pattern to another over time or space, as mentioned by Howard (1967). This author asserts that all transitions are possible from parallel to trellis or dendritic patterns and vice versa. Here, the main transition in drainage patterns in space occur in the north-south or northeast-southwest

direction, from angular pattern in the Saghro and Ougnat inliers (Fig. 11a and b) to trellis patterns in the Bani, MB and OOA sectors (Fig. 11c and d), and then to dendritic patterns in the KKD sector (Fig. 11d). Such transition corresponds to the passage from the Anti-Atlasic domain represented by the SOA sector to the Ougartian domain related to the Ougarta chain. The Ougartian domain interferes with the anti-atlas in the OOA sector, continues under Cretaceous and Neogene formations in the KKD sector, and ends abruptly in the north, crosscut by the Oumjerane-Taouz Fault. It outcrops further in the southeast (Baidder et al., 2016). The transition in time from parallel to trellis pattern can occur during a progressive structural control due to the development of erosion (Howard, 1967). In the western part of the KKD sector, the drainage network is shifting from dendritic to parallel. This may be due to the slow uprising and increase in the slope gradient that have occurred in the EAA since the Lower Mesozoic to the present day (Robert-Charrue, 2006; Jung et al., 2011; Soulaimani et al., 2014; Gouiza et al., 2017). In this structural framework, changes in the orientation of the drainage system over geological time are indicators of transition from one event to another and reflect changes in the factors that control the formation of drainage patterns, as well as transition patterns (Malik and Mohanty, 2007; Brookfield, 2008; Stokes et al., 2008; Radaideh et al., 2016). The principal orientations of the drainage networks (Fig. 9) developed on Precambrian and Paleozoic (NE-SW, NW-SE and E-W) reflect the principal orientations of the geological structures over the entire EAA and mentioned in the literature (Baidder et al., 2016; Bouramtane et al., 2017). They are inherited faults that operated during the collapse of the Pan-African belt and during Cambrian rifting. They have been reactivated as normal faults during the Paleozoic sedimentation and then reversed during the Hercynian event. At the end of the Hercynian event, most of the structure of the Anti-Atlas was established, apart from the reactivation of the inherited faults (Soulaimani et al., 2014). During the Lower Mesozoic and Lower Neogene, the Eastern Anti-Atlas did not record any significant deformation (Robert-Charrue, 2006). However, this period was characterized by a succession of subsidence and uplift events that gave the current topography of the EAA, in particular with higher altitude in the Saghro and Ougnat massifs (Gouiza et al., 2017) and a gradual decrease towards the south and southeast. The directions observed in the rose diagrams for networks developed on the most recent formations rather reflect the influence of the slope gradient. These observations suggest that the drainage system shifts from the influence of structural control in Precambrian and Palaeozoic formations to the influence of topography in the post-Hercynian events from the Lower Mesozoic to the Quaternary. Such observations are consistent with the spatial and temporal transition of the drainage patterns.

5. CONCLUSION

In this work, we have studied the distribution and arrangement of the drainage network in the Eastern Anti-Atlas, an area where the aridity facilitates satellite images of surface formations and drainage networks. We assumed that the patterns of drainage network were not randomly arranged and we looked for factors that could control them. A dataset of 230 basins and 16 parameters related to the topography, morphometry, geology was analyzed by conventional multivariate statistical methods such as principal component analysis (PCA), linear discriminant analysis (LDA) and agglomerative hierarchical clustering (AHC). The number of basins studied is large enough to achieve a reliable statistical approach. The PCA shows that the 16 parameters can be summed up in a rather limited number of independent sources of variability, since the first 6 PCs carry about 86.06% of the information. The number of independent sources of variability (6) is small compared to the number of objects studied (230). Four types of drainage network patterns have been identified, namely trellis, angular, parallel and dendritic patterns. The information contained in this dataset is complex and not redundant. The variation between the different drainage patterns is first explained by parameters related to the topography, the slope and the geology. The LDA made it possible to distinguish between the four types of drainage patterns with a success rate of 90%, using 3 discriminant functions. The dendritic pattern is associated with tabular and homogeneous sedimentary geological formations, little fractured with a small slope gradient. The trellis and angular patterns are associated with geological structures that exhibit intense deformation and fracturing in the study area. They are discriminated based on the distinct geological and geomorphological characteristics of each geological sector. Finally, the parallel pattern network is associated with steeper slopes. Moreover, the similar results from both, the linear discriminant analysis and the unsupervised hierarchical clustering, show confusion and similarity between the parallel, trellis and angular patterns, due to, on the one hand, the similar geological setting responsible for their formation and on the other hand, the possible transition (in time and space) between these three

patterns in the study area. It suggests a possible spatial and temporal transition between the four types of drainage patterns, being the result of a possible shifting of the drainage network, from the influence of structural control in Precambrian and Paleozoic formations, to the influence of topography from post-Hercynian events in the Lower Mesozoic to the Quaternary.

Principal Component Analysis, Linear Discriminant Analysis and agglomerative hierarchical clustering are reference statistical methods, used widely in science. However, the approaches used here suffer from a limitation, in the sense that the data used to search for discriminant functions were calculated on the entire dataset, i.e. on all 230 basins. The discrimination success rate, that is, the validation of the performance of the linear discriminant analysis, is measured on the same set of data using the confusion matrix. A methodological study based on the separation of the data into, on the one hand, a set for the determination of learning methods of the type of drainage patterns from the different parameters, and on the other hand, an independent validation set, would be more in line with a machine learning-type approach. A methodological study to compare the results of these two approaches is currently being carried out and should be presented shortly.

Acknowledgments

This work was carried out in the geoscience, water and environment laboratory of the Faculty of Science of Rabat. It was supported by the National Center for Scientific and Technological Research CNRST within the framework of the Research Excellence Scholarship Program. Jim Hesson of Academic English Solutions (AcademicEnglishSolutions.com) proofread the manuscript.

6. References

Abdelkareem, M., El-Baz, F., 2015. Evidence of drainage reversal in the NE Sahara revealed by space-borne remote sensing data. J. African Earth Sci. 110, 245–257. https://doi.org/https://doi.org/10.1016/j.jafrearsci.2015.06.019

Adiri, Z., Harti, A. El, Jellouli, A., Lhissou, R., Maacha, L., Azmi, M., Zouhair, M., Bachaoui, E.M., 2017. Comparison of Landsat-8, ASTER and Sentinel 1 satellite remote sensing data in automatic lineaments extraction: A case study of Sidi Flah-Bouskour inlier, Moroccan Anti Atlas. Adv. Sp. Res. 60, 2355–2367. https://doi.org/https://doi.org/10.1016/j.asr.2017.09.006

Asfaw, D., Workineh, G., 2019. Quantitative analysis of morphometry on Ribb and Gumara watersheds: Implications for soil and water conservation. Int. Soil Water Conserv. Res. 7, 150–157. https://doi.org/https://doi.org/10.1016/j.iswcr.2019.02.003

Aydogan, D., 2011. Extraction of lineaments from gravity anomaly maps using the gradient calculation: Application to Central Anatolia. Earth, Planets Sp. 63, 903–913. https://doi.org/10.5047/eps.2011.04.003

Babault, J., Van Den Driessche, J., Teixell, A., 2012. Longitudinal to transverse drainage network evolution in the High Atlas (Morocco): The role of tectonics. Tectonics 31. https://doi.org/10.1029/2011TC003015

Baidder, L., Michard, A., Soulaimani, A., Fekkak, A., Eddebbi, A., Rjimati, E.-C., Raddi, Y., 2016. Fold interference pattern in thick-skinned tectonics; a case study from the external Variscan belt of Eastern Anti-Atlas, Morocco. J. African Earth Sci. 119, 204–225. https://doi.org/https://doi.org/10.1016/j.jafrearsci.2016.04.003

Bouramtane, T., Kacimi, I., Saidi, A., Morarech, M., Omari, K., Kassou, N., 2017. Automatic Detection and Evaluation of Geological linear Features from Remote Sensing Data Using the Hough Transform Algorithm in Eastern Anti-Atlas (Morocco), in: 2nd International Conference on Computing and Wireless Communication Systems. ACM New York, Larache, Morocco, pp. 1–6. https://doi.org/10.1145/3167486.3167502

Brookfield, M.E., 2008. Evolution of the great river systems of southern Asia during the Cenozoic India–Asia collision: Rivers draining north from the Pamir syntaxis. Geomorphology 100, 296–311.

https://doi.org/https://doi.org/10.1016/j.geomorph.2008.01.003

Burbank, D.W., Anderson, R.S., 2011. Tectonic Geomorphology, 2. Edition. ed. John Wiley & Sons, Ltd. https://doi.org/10.1002/9781444345063

Burr, D.M., Drummond, S.A., Cartwright, R., Black, B.A., Perron, J.T., 2013. Morphology of fluvial networks on Titan: Evidence for structural control. Icarus 226, 742–759. https://doi.org/https://doi.org/10.1016/j.icarus.2013.06.016

Burrough, P.., McDonnell, R.A., 1998. Principles of Geographical Information Systems, Third Edit. ed. Oxford University Press, New York.

Choubert, G., 1943. Sur le Géorgien de l'Anti-Atlas. C.R. Acad Sci, Paris 216, 69–70.

Choubert, G., Faure-Muret, A., Destombes, J., 1989. Carte Geologique du Maroc au 1/200 000, feuille Zagora-Coude du Dra-Hamada du Dra. Notes et Memoires du Service Geologique du Maroc, 273.

Clariond, L., Choubert, G., Lavocat, R., Joly, F., Poueyto, A., 1982. Carte Geologique du Maroc au 1/200 000, feuille BOU Haiara-Zegdou. Notes et Memoires du Service Geologique du Maroc, 259.

Clark, M.K., Schoenbohm, L.M., Royden, L.H., Whipple, K.X., Burchfiel, B.C., Zhang, X., Tang, W., Wang, E., Chen, L., 2004. Surface uplift, tectonics, and erosion of eastern Tibet from large-scale drainage patterns. Tectonics 23. https://doi.org/10.1029/2002TC001402

Clarke, J.D.A., 1994. Evolution of the Lefroy and Cowan palaeodrainage channels, Western Australia. Aust. J. Earth Sci. 41, 55–68. https://doi.org/10.1080/08120099408728113

Colmenar, J., Villas, E., Rasmussen, C.M.Ø., 2018. A synopsis of Late Ordovician brachiopod diversity in the Anti-Atlas, Morocco. Geol. Soc. London, Spec. Publ. 485. https://doi.org/10.1144/SP485.3

Day, D.G., 1980. Lithologic controls of drainage density: A study of six small rural catchments in New England, N.S.W. CATENA 7, 339–351. https://doi.org/https://doi.org/10.1016/S0341-8162(80)80024-5

Demoulin, A., 1998. Testing the tectonic significance of some parameters of longitudinal river profiles: the case of the Ardenne (Belgium, NW Europe). Geomorphology 24, 189–208. https://doi.org/https://doi.org/10.1016/S0169-555X(98)00016-6

Destombes, J., Hollard, H., 1986. Carte Geologique du Maroc au 1/200 000, feuille TafilalteTaouz. Notes et Memoires du Service Geologique du Maroc, 244.

Drury, S.A., 2004. Image interpretation in Geology, 3rd editio. ed. Taylor & Francis, Inc., Cheltenham.

Du Dresnay, R., Hindermeyer, J., Emberger, A., Gaia, J., Destombes, J., Hollard, H., 1988. Carte Geologique du Maroc au 1/200 000, feuille Todrgha-Ma'der. Notes et Memoires du Service Geologique du Maroc, 243.

Fal, S., Maanan, M., Baidder, L., Rhinane, H., 2019. The contribution of Sentinel-2 satellite images for geological mapping in the south of Tafilalet Basin (Eastern Anti-Atlas, Morocco). ISPRS - Int. Arch. Photogramm. Remote Sens. Spat. Inf. Sci. XLII-4/W12, 75–82. https://doi.org/10.5194/isprs-archives-XLII-4-W12-75-2019

Fels, A.E.A. El, Alaa, N., Bachnou, A., Rachidi, S., 2018. Flood frequency analysis and generation of flood hazard indicator maps in a semi-arid environment, case of Ourika watershed (western High Atlas, Morocco). J. African Earth Sci. 141, 94–106. https://doi.org/https://doi.org/10.1016/j.jafrearsci.2018.02.004

Fink, A.H., Knippertz, P., 2003. An extreme precipitation event in southern Morocco in spring 2002 and some hydrological implications. Weather 58, 377–387. https://doi.org/10.1256/wea.256.02

Friend, P.F., Jones, N.E., Vincent, S.J., 2009. Drainage Evolution in Active Mountain Belts: Extrapolation Backwards from Present-Day Himalayan River Patterns, in: Fluvial Sedimentology VI. John Wiley & Sons, Ltd, pp. 305–313. https://doi.org/10.1002/9781444304213.ch22

Frizon de Lamotte, D., Zizi, M., Missenard, Y., Hafid, M., Azzouzi, M. El, Maury, R.C., Charrière, A., Taki, Z., Benammi, M., Michard, A, 2008. The Atlas System BT - Continental Evolution: The Geology of Morocco: Structure, Stratigraphy, and Tectonics of the Africa-Atlantic-Mediterranean Triple Junction, in: Michard, André, Saddiqi, O., Chalouan, A., Lamotte, D.F. de (Eds.), . Springer Berlin Heidelberg, Berlin, Heidelberg, pp. 133–202. https://doi.org/10.1007/978-3-540-77076-3_4

Gouiza, M., Charton, R., Bertotti, G., Andriessen, P., Storms, J.E.A., 2017. Post-Variscan evolution of the Anti-Atlas belt of Morocco constrained from low-temperature geochronology. Int. J. Earth Sci. 106, 593–616. https://doi.org/10.1007/s00531-016-1325-0

Gunkel, A., Shadeed, S., Hartmann, A., Wagener, T., Lange, J., 2015. Model signatures and aridity indices enhance the accuracy of water balance estimations in a data-scarce Eastern Mediterranean catchment. J. Hydrol. Reg. Stud. 4, 487–501. https://doi.org/https://doi.org/10.1016/j.ejrh.2015.08.002

Hefferan, K., Soulaimani, A., Samson, S.D., Admou, H., Inglis, J., Saquaque, A., Latifa, C., Heywood, N., 2014. A reconsideration of Pan African orogenic cycle in the Anti-Atlas Mountains, Morocco. J. African Earth Sci. 98, 34–46. https://doi.org/https://doi.org/10.1016/j.jafrearsci.2014.03.007

Hilali, M., 2015. Hydrogéologie et ressources en eau du Tafilalet et ses régions limitrophes (sud-est du Maroc): connaissance, prospection, caractérisation, exploitation et gestion des ressources en eau. Mohamed V University Rabat.

Hinderleyer, J., Gauthier, H., Destombes, J., Choubert, G., Faure-Muret, A., Laville, E., Lesage, J.-L., Du Dresnay, R., 1977. Carte Geologique du Maroc au 1/200 000, feuille Jbel Saghro-Dades. Notes et Memoires du Service Geologique du Maroc, 161.

Horton, R.E., 1932. Drainage-basin characteristics. Eos, Trans. Am. Geophys. Union 13, 350–361. https://doi.org/10.1029/TR013i001p00350

Horton, R.E., 1942. Remarks on hydrologic terminology. Trans. Am. Geophys. Union 23, 479–482.

Howard, A.D., 1967. Drainage Analysis in Geologic Interpretation: A Summation. Am. Assoc. Pet. Geol. Bull. 51, 2246–2259.

El Janati, M. (2019). Application of remotely sensed ASTER data in detecting alteration hosting Cu, Ag and Au bearing mineralized zones in Taghdout area, Central Anti-Atlas of Morocco. *Journal of African Earth Sciences*, *151*, 95-106.

Johnson, D., 1932. Streams and Their Significance. J. Geol. 40, 481–497. https://doi.org/10.1086/623975

Jung, K., Niemann, J.D., Huang, X., 2011. Under what conditions do parallel river networks occur? Geomorphology 132, 260–271. https://doi.org/https://doi.org/10.1016/j.geomorph.2011.05.014

Jung, K., Ouarda, T.B.M.J., 2017. Classification of drainage network types in the arid and semi-arid regions of Arizona and California. J. Arid Environ. 144, 60–73. https://doi.org/https://doi.org/10.1016/j.jaridenv.2017.04.013

Jung, K., Shin, J.-Y., Park, D., 2019. A new approach for river network classification based on the beta distribution of tributary junction angles. J. Hydrol. 572, 66–74. https://doi.org/https://doi.org/10.1016/j.jhydrol.2019.02.041

Karnieli, A., Meisels, A., Fisher, L., Arkin, Y., 1996. Automatic Extraction and Evaluation of Geological Linear Features from Digital Remote Sensing Data Using a Hough Transform. Photogramm. Eng. Remote

Sensing, 62, 525–531.

Kassou, N., 2016. Hydrogéologie, hydrogéochimie et qualité des eaux des nappes aquifères du bassin de l'Oued Reg, région d'Alnif Anti-Atlas Oriental. Mohamed V University, Rabat.

Kaufmann, B., 1998. Middle Devonian reef and mud mounds on a carbonate ramp: Mader Basin (eastern Anti-Atlas, Morocco). Geol. Soc. London, Spec. Publ. 149, 417–435. https://doi.org/10.1144/GSL.SP.1999.149.01.19

Langbein, W.B., 1964. Profiles of rivers of uniform discharge. United States Geol. Surv. Prof. Pap. 501, 119–122.

Malik, J.N., Mohanty, C., 2007. Active tectonic influence on the evolution of drainage and landscape: Geomorphic signatures from frontal and hinterland areas along the Northwestern Himalaya, India. J. Asian Earth Sci. 29, 604–618. https://doi.org/https://doi.org/10.1016/j.jseaes.2006.03.010

Mejía, A.I., Niemann, J.D., 2008. Identification and characterization of dendritic, parallel, pinnate, rectangular, and trellis networks based on deviations from planform self-similarity. J. Geophys. Res. Earth Surf. 113, 1–21. https://doi.org/10.1029/2007JF000781

Melton, M.A., 1957. An analysis of the relations among elements of climate, surface properties, and geomorphology, Technical. ed. Columbia Univ., New York.

Mengistu, A.G., van Rensburg, L.D., Woyessa, Y.E., 2019. Techniques for calibration and validation of SWAT model in data scarce arid and semi-arid catchments in South Africa. J. Hydrol. Reg. Stud. 25, 100621. https://doi.org/https://doi.org/10.1016/j.ejrh.2019.100621

Mohammadi, A., Costelloe, J.F., Ryu, D., 2017. Application of time series of remotely sensed normalized difference water, vegetation and moisture indices in characterizing flood dynamics of large-scale arid zone floodplains. Remote Sens. Environ. 190, 70–82. https://doi.org/https://doi.org/10.1016/j.rse.2016.12.003

Mueller, E.R., Pitlick, J., 2013. Sediment supply and channel morphology in mountain river systems: 1. Relative importance of lithology, topography, and climate. J. Geophys. Res. Earth Surf. 118, 2325–2342. https://doi.org/10.1002/2013JF002843

Ouanaimi, H., Soulaimani, A., Baidder, L., Eddebbi, A., Hoepffner, C., 2018. Unraveling a distal segment of the West African Craton Paleozoic margin: Stratigraphy of the Mougueur inlier of the eastern High Atlas, Morocco. Comptes Rendus Geosci. 350, 289–298. https://doi.org/https://doi.org/10.1016/j.crte.2018.06.008

Ouarda, T.B.M.J., Jung, K., 2015. Analysis and Classification of Channel Network Types for Intermittent Streams in the United Arab Emirates and Oman. J. Civ. Environ. Eng. 05. https://doi.org/10.4172/2165-784x.1000183

Parvis, M., 1950. Drainage pattern significance in airphoto identification of soils and bedrocks. Photogramm. Eng. 16, 375–409.

Pereira-Claren, A., Gironás, J., Niemann, J.D., Passalacqua, P., Mejia, A., Escauriaza, C., 2019. Planform geometry and relief characterization of drainage networks in high-relief environments: An analysis of Chilean Andean basins. Geomorphology 341, 46–64. https://doi.org/https://doi.org/10.1016/j.geomorph.2019.05.011

Poncelet, N., Cornet, Y., 2010. Transformée de Hough et détection de linéaments sur images satellitaires et modèles numériques de terrain. Bull. la Société Géographique Liège 54, 145–155.

Radaideh, O.M.A., Grasemann, B., Melichar, R., Mosar, J., 2016. Detection and analysis of morphotectonic

features utilizing satellite remote sensing and GIS: An example in SW Jordan. Geomorphology 275, 58–79. https://doi.org/https://doi.org/10.1016/j.geomorph.2016.09.033

Rawat, K.S., Mishra, A.K., Tripathi, V.K., 2013. Hydro-morphometrical analyses of sub-himalyan region in relation to small hydro-electric power. Arab. J. Geosci. 6, 2889–2899. https://doi.org/10.1007/s12517-012-0586-6

Renson, P., Poncelet, N., Vandeloise, Y., Schmidt, R., Cornet, Y., 2013. Automatisation de la détection des cratères lunaires sur des images et MNT planétaires. Bull. la Société Géographique Liège 61, 81–96.

Rezende-Filho, A.T., Valles, V., Furian, S., Oliveira, C.M.S.C., Ouardi, J., Barbiero, L., 2015. Impacts of lithological and anthropogenic factors affecting water chemistry in the upper Paraguay River Basin. J. Environ. Qual. 44. https://doi.org/10.2134/jeq2015.01.0019

Robert-Charrue, 2006. Géologie structurale de l'Anti-Atlas oriental. Neuchâtel University.

Saidi, M.E., 1994. Genèse et propagation des crues en milieu sub-aride : exemple de l ' Oued Souss (Maroc) (Flood's genesis and propagation in sub-arid environment as exemplified by Oued Souss (Morrocco)). Bull. Assoc. Geogr. Fr. 71, 94–111.

Sangireddy, H., Carothers, R.A., Stark, C.P., Passalacqua, P., 2016. Controls of climate, topography, vegetation, and lithology on drainage density extracted from high resolution topography data. J. Hydrol. 537, 271–282. https://doi.org/https://doi.org/10.1016/j.jhydrol.2016.02.051

Schumm, S.A., 1956. Evolution of drainage systems and slopes in badlands at Perth Amboy, New Jersey. GSA Bull. 67, 597–646. https://doi.org/10.1130/0016-7606(1956)67[597:EODSAS]2.0.CO;2

Schumm, S.A., Dumont, J.F., Holbrook, J.M., 2002. Active tectonics and alluvial rivers. Cambridge University Press, New York.

Soulaimani, A., Michard, A., Ouanaimi, H., Baidder, L., Raddi, Y., Saddiqi, O., Rjimati, E.C., 2014. Late Ediacaran–Cambrian structures and their reactivation during the Variscan and Alpine cycles in the Anti-Atlas (Morocco). J. African Earth Sci. 98, 94–112. https://doi.org/https://doi.org/10.1016/j.jafrearsci.2014.04.025

Stokes, M., Mather, A.E., Belfoul, A., Farik, F., 2008. Active and passive tectonic controls for transverse drainage and river gorge development in a collisional mountain belt (Dades Gorges, High Atlas Mountains, Morocco). Geomorphology 102, 2–20. https://doi.org/https://doi.org/10.1016/j.geomorph.2007.06.015

Strahler, A.N., 1954. Statistical Analysis in Geomorphic Research. J. Geol. 62, 1–25.

Twidale, C.R., 1994. Gondwanan (Late Jurassic and Cretaceous) palaeosurfaces of the Australian craton. Palaeogeogr. Palaeoclimatol. Palaeoecol. 112, 157–186. https://doi.org/https://doi.org/10.1016/0031-0182(94)90139-2

Twidale, C.R., 1997. Persistent and ancient rivers - Some Australian examples. Phys. Geogr. 18, 291–317. https://doi.org/10.1080/02723646.1997.10642621

Twidale, C.R., 2004. River patterns and their meaning. Earth-Science Rev. 67, 159–218. https://doi.org/https://doi.org/10.1016/j.earscirev.2004.03.001

Van der Meer, F.D., Van der Werff, H.M.A., Van Ruitenbeek, F.J.A., 2014. Potential of ESA's Sentinel-2 for geological applications. Remote Sens. Environ. 148, 124–133. https://doi.org/https://doi.org/10.1016/j.rse.2014.03.022

Walsh, G.J., Benziane, F., Aleinikoff, J.N., Harrison, R.W., Yazidi, A., Burton, W.C., Quick, J.E., Saadane, A.,

2012. Neoproterozoic tectonic evolution of the Jebel Saghro and Bou Azzer—El Graara inliers, eastern and central Anti-Atlas, Morocco. Precambrian Res. 216–219, 23–62. https://doi.org/https://doi.org/10.1016/j.precamres.2012.06.010

Zernitz, E.R., 1932. Drainage Patterns and Their Significance. J. Geol. 40, 498–521. https://doi.org/10.1086/623976